Influence of InP Coupling Cavity on Fano Resonance of Sub Wavelength MIM Waveguide

Shihao Ban

School of Physics and Electronics of Hunan University

Huangqing Liu (✉ lhq468@sohu.com)

School of Physics and Electronics of Hunan University

Shifang Xiao

School of Physics and Electronics of Hunan University

Jingjing Mao

Huaihua Normal College

Jie Luo

Central South University of Forestry and Technology

Research Article

Abstract

In this paper, influence of InP coupling cavity (height H_2) on Fano resonance of sub wavelength MIM waveguide was studied by FDTD. It was observed redshift of the resonance peaks of mode m_j (j=1, 2, 3) with H_2 increase and the resonant wavelengths of mode m_j (j=1, 2, 3) were a function of the height H_2. Before and after the addition of air cavity, the relative farfield intensities I was a function of height H_2. Therefore, InP as discrete state would be used as the filling dielectrics of Fano resonance in the MIM waveguide.

Background

Due to its attractive features and extensive applications, the metal−insulator−metal (MIM) waveguide [1-5] were very popular with researchers. During the process of light propagation in the nano-photonic circuits, MIM waveguides could reduce energy loss. The MIM waveguide with coupling cavity introduced into could change its filtering performance of electromagnetic wave[6-9], such as Fano resonance. The most common structures of the plasmonic filters were MIM waveguides coupled with a rectangular cavity[10-12]. There were some researches on the Fano resonance of silicon in the coupling cavity of MIM waveguides[13-14]. Due to relatively large dielectric constant and high-order resonance about 1700 nm in the near-infrared region, silicon was usually regarded as discrete state of Fano resonance[13-18]. In addition, in the study, obvious Fano resonance over 2100nm was observed when the dielectrics were InP in the coupling cavity of MIM waveguide. In other words, InP could also be used as discrete state of Fano resonance. Compared with silicon, due to better radiation resistance and higher cut-off frequencies, InP could be chemically etched to make radiation resistant devices and be applied in solar cells[19-21] and semiconductor optoelectronic devices[22-24]. Therefore, InP as discrete state of Fano resonance[25] would be used as the filling dielectrics in the MIM waveguide and the influence of InP coupling cavity on Fano resonance of sub wavelength MIM waveguide (Ag-Air-Ag) was explored in this paper.

Results

The sketch of the waveguide structure designed was shown in Fig. 1. In the figure, the distance w of the main waveguide cavity with the transparent dielectrics (n=1.0) was set as 50 nm which was far less than the wavelength λ of incident wave from 600 nm to 2700 nm so that the electromagnetic wave could be excited to form SPPs propagation mode in MIM waveguide structure. After that, a j-order (j=1, 2 and 3) resonance formed when the coupled cavity was excited by the main waveguide, whose width L of the coupled cavities was also set as 50 nm. Our simulation results indicated that Fano resonance was independent of the horizontal distance between the two cavities and dependent on the height H_1 (H_2). In addition, the relative far-field intensity I was defined as the area under the far-field curve and was proportional to the height h of the curve in this paper.

Fig.2a showed the transmission spectra under different InP structures without air cavity A. It could be observed redshift of the resonance peaks of mode m_j (j=1,2,3) with the increase of H_2 from 240 nm to 350 nm. The resonant wavelengths of mode m_j (j=1, 2, 3) were a function of the height H_2. Take H_2=350 nm as an example, it was observed three resonance valleys at 998 nm, 1302 nm and 2079 nm, respectively. The resonance valleys at 1302 nm and 2079 nm were first and second order resonance modes, shown in Fig. 2(c-d). However, the resonance valley at 998 nm was located at the critical point of the second and third order resonance and was regarded as third-order resonance, seen in Fig. 2(a-b). In other words, the resonance mode in Fig. 2a could directly be reflected by the distribution of magnetic field in Fig. 2(b-d).

In addition, when the zero order dark mode from the Air cavity and j-order bright modes (j=1, 2 and 3) from the InP cavity were superimposed, some Fano resonance of the modes m_j (j=1, 2 and 3) could be obtained in Fig.3a, which showed the transmission spectra of different InP-Air structures whose structural parameters were H_1=300 nm and various H_2. In the case of only air cavity, it could be observed that the transmission spectrum was very wide passband, which covered the resonance wavelengths of the modes m_j (j=1, 2 and 3) and whose central wavelength was at about 1710 nm. Therefore, for the mode m_1, it was observed no Fano resonance when H_2=280 nm and 300 nm, two slightly obvious Fano resonances when H_2=320 nm and 350 nm in the range from 1800 nm to 2700 nm (not marked), and more obvious Fano resonance when H_2=240 nm and 260 nm. However, the most obvious Fano resonance came from the mode m_2 whose resonance valley shifted to the long wavelength with the H_2 increase. According to the main resonance peak [22-23] of the mode m_2 in the figure 3a, the quality factor (QF) and the extinction ratio (ER) could be calculated. A high-quality factor was meant to be lower light energy loss in a resonant cavity. Moreover, the lager extinction ratio was implied the better quality of the resonator. For the different InP-Air structures with the length H_2 from 240 nm to 350 nm (240 nm, 260 nm, 280 nm, 300 nm, 320 nm and 350 nm), the quality factor QFs calculated were about 44, 30, 29, 28, 34 and 37 respectively. The ERs obtained were around 13, 18, 15, 14, 31 and 12 dB, respectively.

These results showed that the QFs and the ERs were a function of the length H_2. There was lower light energy loss in a resonant cavity and the better quality of the resonator for the length H_2=240nm and 320nm. In other words, when the height H_2 was not higher than 240 nm and not less than 320 nm, the waveguide structure with InP-Air cavities had good filtering performance. In addition, it was obtained that the addition of air cavity did not change the position of the resonant valleys which was dependent on structure sizes of the cavity InP. Take H_2=350 nm as an example, for the three resonance valleys at 998 nm, 1302 nm and 2079 nm, it was observed the magnetic field distribution did not change before and after the addition of air cavity. Additionally, it was obtained that the magnetic field distribution of the zero-order resonance in the air cavity where no standing wave was observed, as shown in Fig. 3(b-d).

Figure 4 showed the relationship between transmission and the height H_1. The structural parameter was H_2=260 nm. It was observed that the resonance position of the mode m_j (j=1, 2 and 3) was independent

of the height H_1. The broadband resonances between 1500nm and 2100nm were considered to originate zero-order resonance of air cavity, which moved to the long wavelength with H_1 increasing. In addition, because of strong resonance of the zero-order mode the resonance of mode m_1 was barely observed when $H_1 < 280$nm. However, the intensity of resonance peak at about 1645nm gradually decreased with the increment of H_1 (>300nm). The QF and the ER were about up to 37 and 16 dB when $H_1 = 350$nm. Nevertheless, by the simulation, we obtained that the QF and ER decreased to 29 and 14dB when $H_1 = 360$ nm.

Before the addition of air cavity, under 1302.87 nm monitoring, the relative farfield intensities I were various with the height H_2 change from 240 nm to 350 nm and was a function of height H_2, namely, $I = I(H_2)$, as shown in Fig.5a. The shape of the curve was Guassian Spot with periodic structure, whose symmetric center was located at about $\theta = -2.2^0$, as shown in the black dash. The relative farfield intensity I gradually decreased with the height H_2 from 260 nm to 350 nm. The maximum relative intensity $I(260)$ was about three times that of the minimum $I(350)$, $I(260) = 3I(350)$. After the addition of air cavity, it was observed that the relative farfield intensities I was also a function of height H_2, as shown in Fig. 5b. The symmetric center of the curve with periodic structure was located at about $\theta = 0^0$, as seen in the black dash. The relative farfield intensity I gradually increased with the height H_2 from 240 nm to 320 nm. The maximum relative intensity $I(320)$ was about four times that of the minimum $I(350)$, namely, $I(320) = 4I(350)$. Therefore, the change of structural parameters could be obtained according to the change of far-field relative intensity [20].

Discussion

Influence of InP coupling cavitftably (height H_2) on Fano resonance of sub wavelength MIM waveguide was studied in this paper. Some novel results were obtained. For different InP structures without air cavity, it was observed redshift of the resonance peaks of mode m_j (j=1, 2 and 3) with H_2 increase and the resonant wavelengths of mode m_j (j=1, 2 and 3) were a function of the height H_2. For the different InP-Air structures with the length H_2 from 240 nm to 350 nm, the resonance valley of the mode m_2 shifted to the long wavelength with the H_2 increase. For the structural parameter $H_2 = 260$ nm, the resonance position of the mode m_j (j=1, 2 and 3) was independent of the height H_1. In addition, before and after the addition of air cavity, the relative farfield intensities I was a function of height H_2. Therefore, InP as discrete state of Fano resonance would be used as the filling dielectrics of Fano resonance in the MIM waveguide.

Methods

Numerical simulations. In the letter, the MIM plasmonic waveguide coupled with InP cavity was investigated using the finite-difference time-domain (FDTD, Lumerical Computational Solutions Incorporation) with a perfectly matched layer absorbing boundary condition. A plane wave with the

electric field parallel to the x axis illuminates normally the periodic structure. The grid sizes in the x and y directions were 2 nm.

Declarations

Acknowledgements

Authors' contributions

H.Q.L wrote the article and participated in the analysis and interpretation of the data. S.H. B and J.J. M participated in part of the study design and interpretation of the data. S.F.X and J. L provided financial support.

Additional Information

Author information: School of Physics and Electronics, Hunan University, Changsha 410082, PR China, S. Ban, H. Liu & S. Xiao; **Huaihua Normal College, Huaihua 418008, PR China,** Jingjing Mao; **School of Material Science and Engineering, Central South University of Forestry and Technology, 410004, Hunan, PR China,** Jie Luo.

Corresponding author: Correspondence to H. Liu (lhq468@sohu.com) & J. Mao (**mjj6937213@163.com**).

Conflicts of interest: The authors declared that they had no conflict of interest.

Ethics approval: This work was carried out in accordance with the principles outlined in the journal's ethical policy and informed consent to publish was obtained from all participants.

References

1. P. Törmä & W. L. Barnes, Strong coupling between surface plasmon polaritons and emitters: a review, *Rep. Prog. Phys.* **78** 013901(2015).
2. S. O. Abdol, etal., Tunable surface plasmon polaritons in a Weyl semimetal waveguide, *J. Phys.: Condens. Matter* **31** 335002(2019).
3. Ž. B. Lošić, Surface plasmons in Weyl semimetals, *J. Phys.: Condens. Matter* **30** 365003 (2018).
4. N. M. Saleh & A. A. Aziz, Simulation of Surface Plasmon Resonance on Different Size of a Single Gold Nanoparticle, *Journal of Physics: Conf. Series* **1083** 012041 (2018).
5. E. Cao, etal., Exciton−plasmon hybrids for surface catalysis detected by SERS, *Nanotechnology* **29** 372001 (2018).

6. G. A. Melentev, etal., Surface plasmon-phonon polaritons in GaAs, *Journal of Physics: Conf. Series* **917** 062038 (2017).

7. Y. Kim, etal., Demonstration of integrated polarization rotator based on an asymmetric silicon waveguide with a trench, *J. Opt.* **18** 095801 (2016).

8. S. Ghosh, etal., Transverse localization of light in 1D disordered waveguide lattices in the presence of a photonic bandgap, *Laser Phys.* **24** 045001 (2014).

9. B. Piccione, etal., Tailoring light–matter coupling in semiconductor and hybrid-plasmonic nanowires, *Rep. Prog. Phys.* **77** 086401 (2014).

10. K. Wen, etal., Wavelength demultiplexing structure based on a plasmonic metal−insulator−metal waveguide, *J. Opt.* **14** 075001 (2012).

11. Y. Sheng, etal., Fabrication of lateral electrodes on semiconductor nanowires through structurally matched insulation for functional optoelectronics, *Nanotechnology* **24** 025204 (2013).

12. B. Yun, G. Hu, C. J. Wei, Plasmon induced transparency in metal−insulator−metal waveguide by a stub coupled with F-P resonator, *Materials Research Express* **1** 036201 (2014).

13. X. Zhong, Z. Li, Plasmon enhanced light amplification in metal−insulator−metal waveguides with gain, *J. Opt.* **14** 055002 (2012).

14. Y. Wang, X. Yan, Mode conversion in metal−insulator−metal waveguide with a shifted cavity, *Japanese Journal of Applied Physics* **57** 010303 (2018).

15. G. Zheng, W. Su, Y. Chen, Band-stop filters based on a coupled circular ring metal−insulator−metal resonator containing nonlinear material, *J. Opt.* **14** 055001(2012).

16. T. Nurmohammadi , etal. Ultra-fast all-optical plasmon induced transparency in a metal−insulator−metal waveguide containing two Kerr nonlinear ring resonators, *J. Opt.* **20** 055504 (2018).

17. B. Yun, G. Hu, Y. Cui, Theoretical analysis of a nanoscale plasmonic filter based on a rectangular metal−insulator−metal waveguide, *J. Phys. D: Appl. Phys.* **43** 385102 (2010).

18. S. Li, H. Liu , L. Liu, Effect of silver film thickness on the surface plasma resonance in the rectangular Ag-Si-SiO$_2$ cavity, *J. Phys. Commun.* **2** 055024 (2018).

19. S. Li, etal. Investigation of Surface Plasmon Resonance in the Rectangular Cavity of Ag-Si-SiO$_2$, *Plasmonics*, **13**(6) 2313 (2018).

20. S. Li, etal. Farfield Under Small Scattering Angle in the Rectangular Ag−Si−SiO$_2$ Cavity , *Plasmonics* **14** 1385 (2019).

21. S. Ghorbani, M. A. Dashti, M. Jabbar, Plasmonic nano-sensor based on metal-dielectric-metal waveguide with the octagonal cavity ring, *Laser Phys.* **28** 066208 (2018).

22. J Mao, etal. Numerical analysis of near-infrared plasmonic filter with high figure of merit based on Fano resonance, *Applied Physics Express* **10** 082201 (2017).

23. S. Zhang, G. Li, Y. Chen, Pronounced Fano Resonance in Single Gold Split Nanodisks with 15 nm Split Gaps for Intensive Second Harmonic Generation, *ACS Nano* **10** 11105 (2016).
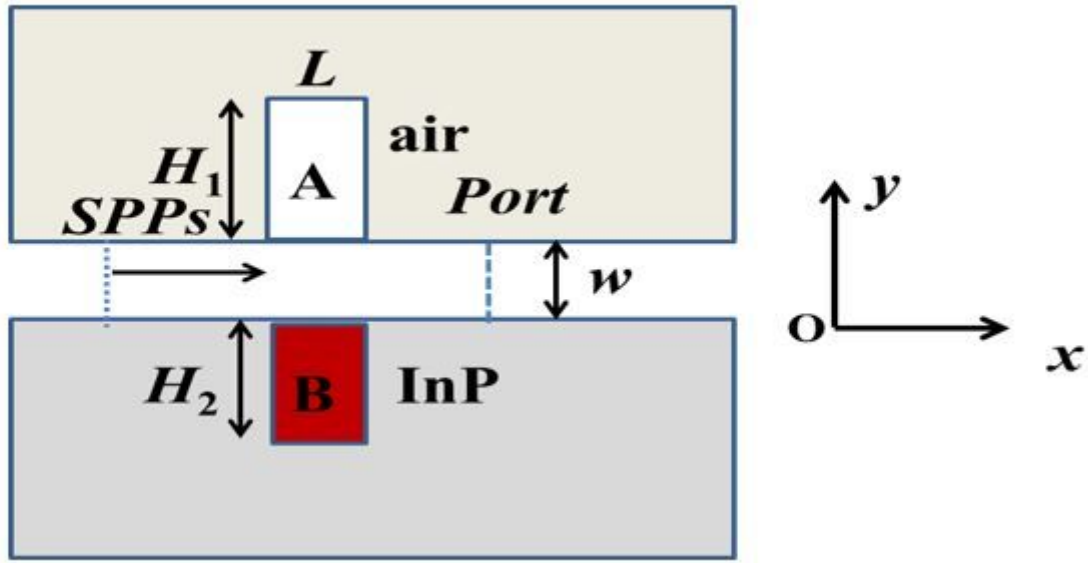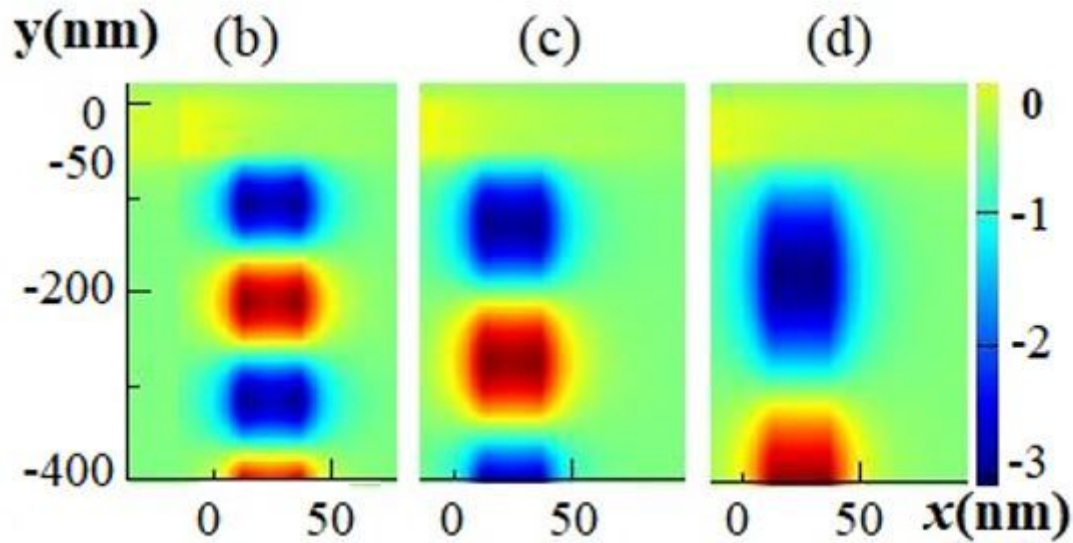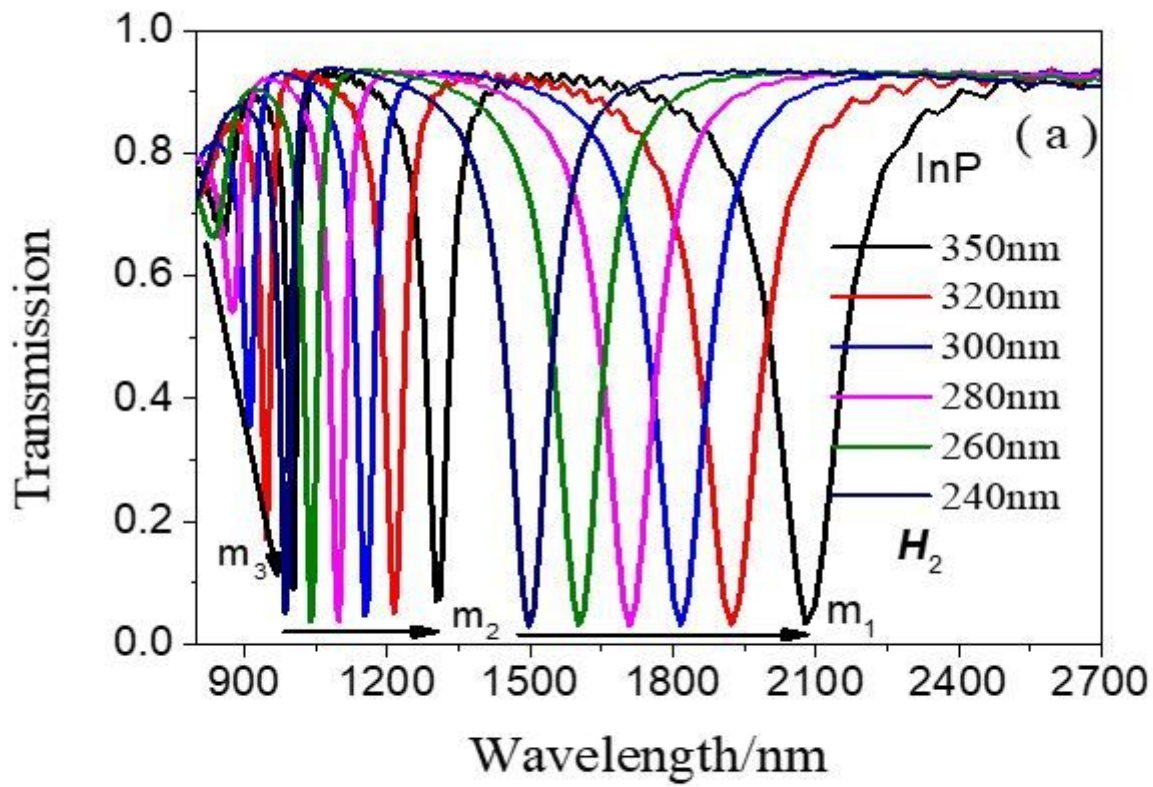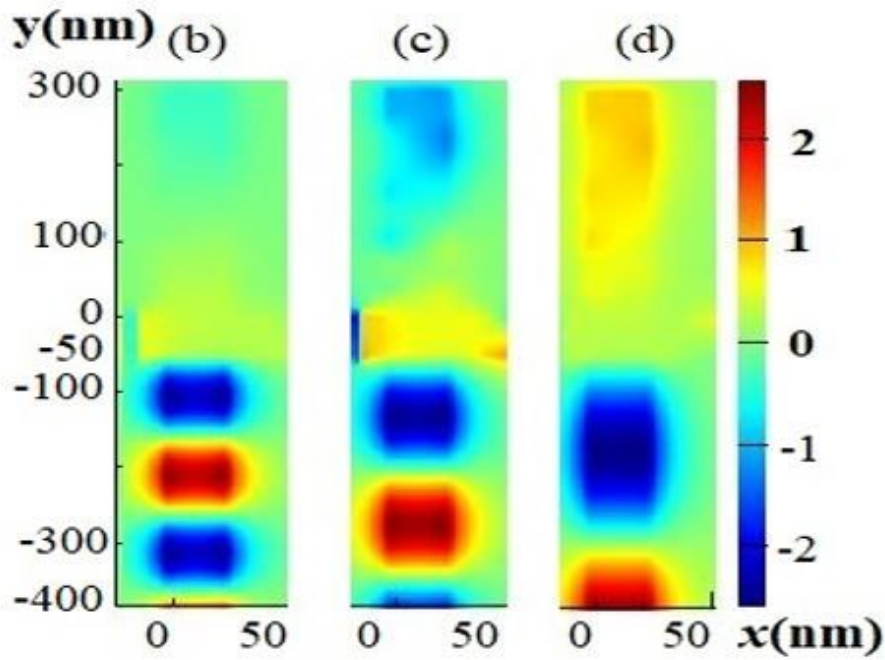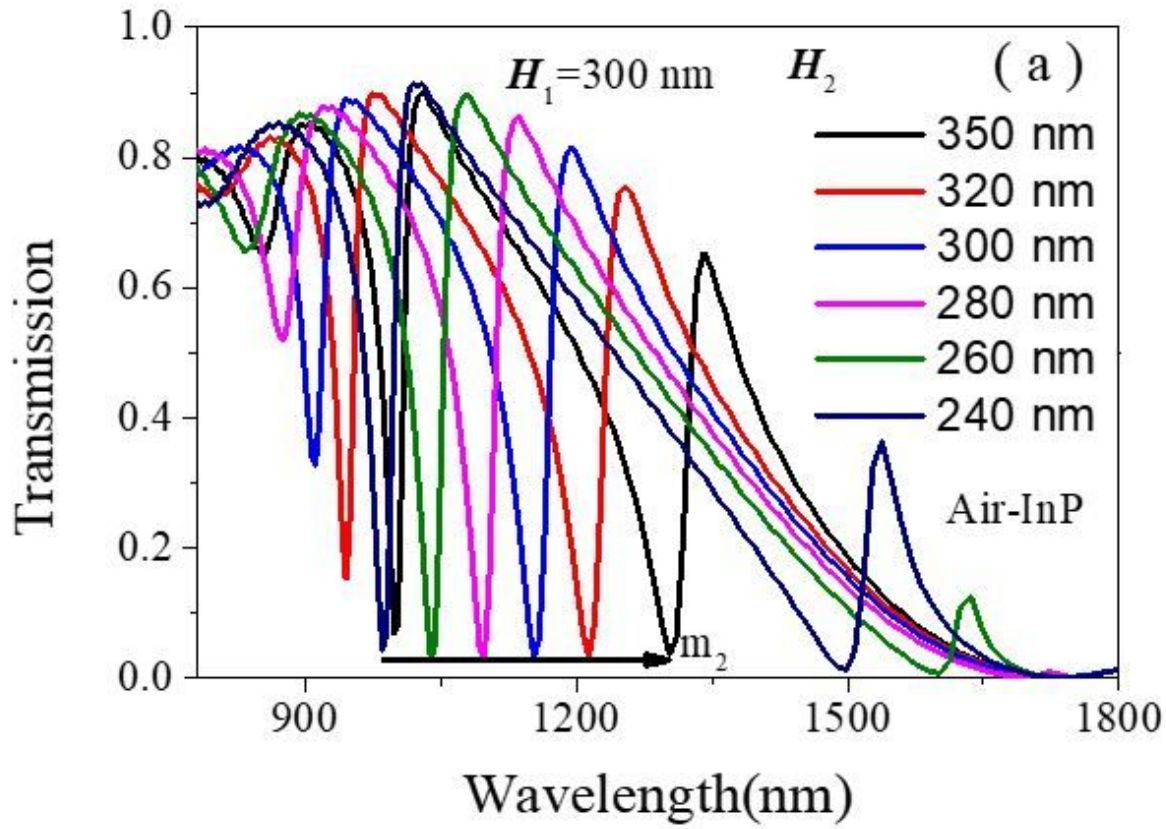
Figures

Figure 1

Research scheme and design schematic of 2D simulation. The capital letters A and B denote air and InP coupled cavities, respectively. The structural parameters were L=w=50nm.
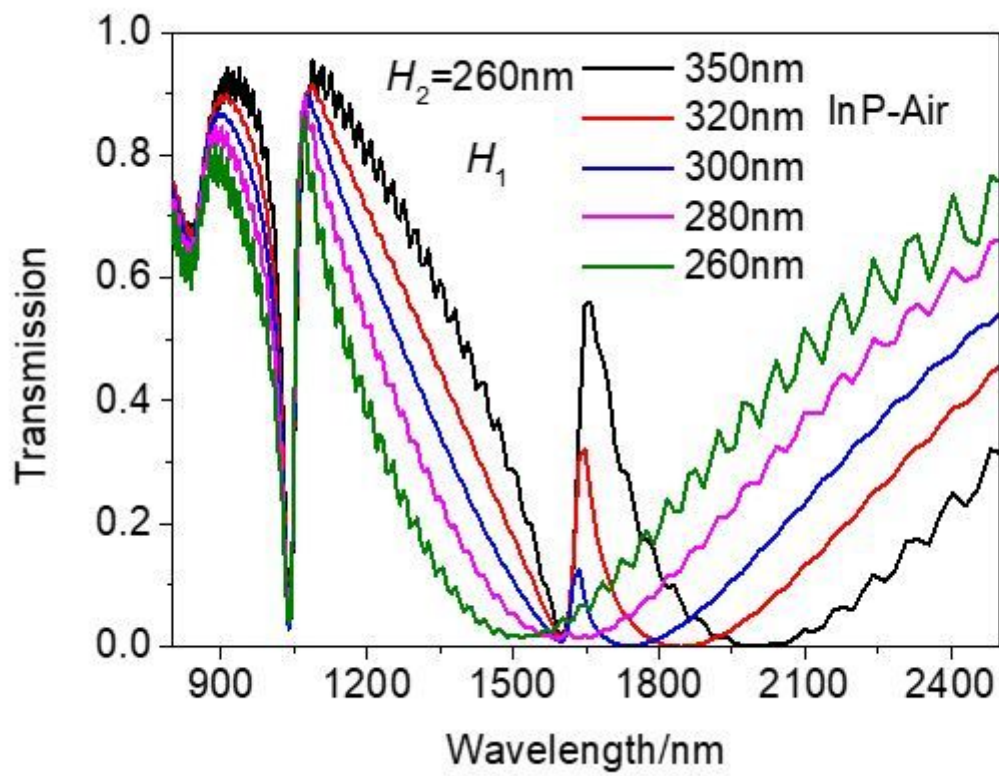
Figure 2

(a)The relation between Fano resonance and the height H2. (b)(c)(d) Magnetic field distribution of different modes at different resonance wavelengths 998 nm, 1302 nm and 2079 nm, respectively. Red and blue represent two different vibrations. The structural parameter was H2=350 nm.

Figure 3

(a) The relationship between Fano resonance and the height H2 in the range from 780 nm to 1800 nm. (b)(c)(d) Magnetic field distribution of different modes at different resonance wavelengths 998 nm, 1302 nm and 2079 nm, respectively. Red and blue represent two different vibrations. The structural parameter was H1=300 nm.

Figure 4

The relationship between transmission and the height H1. The structural parameters were H2=260nm .

Figure 5

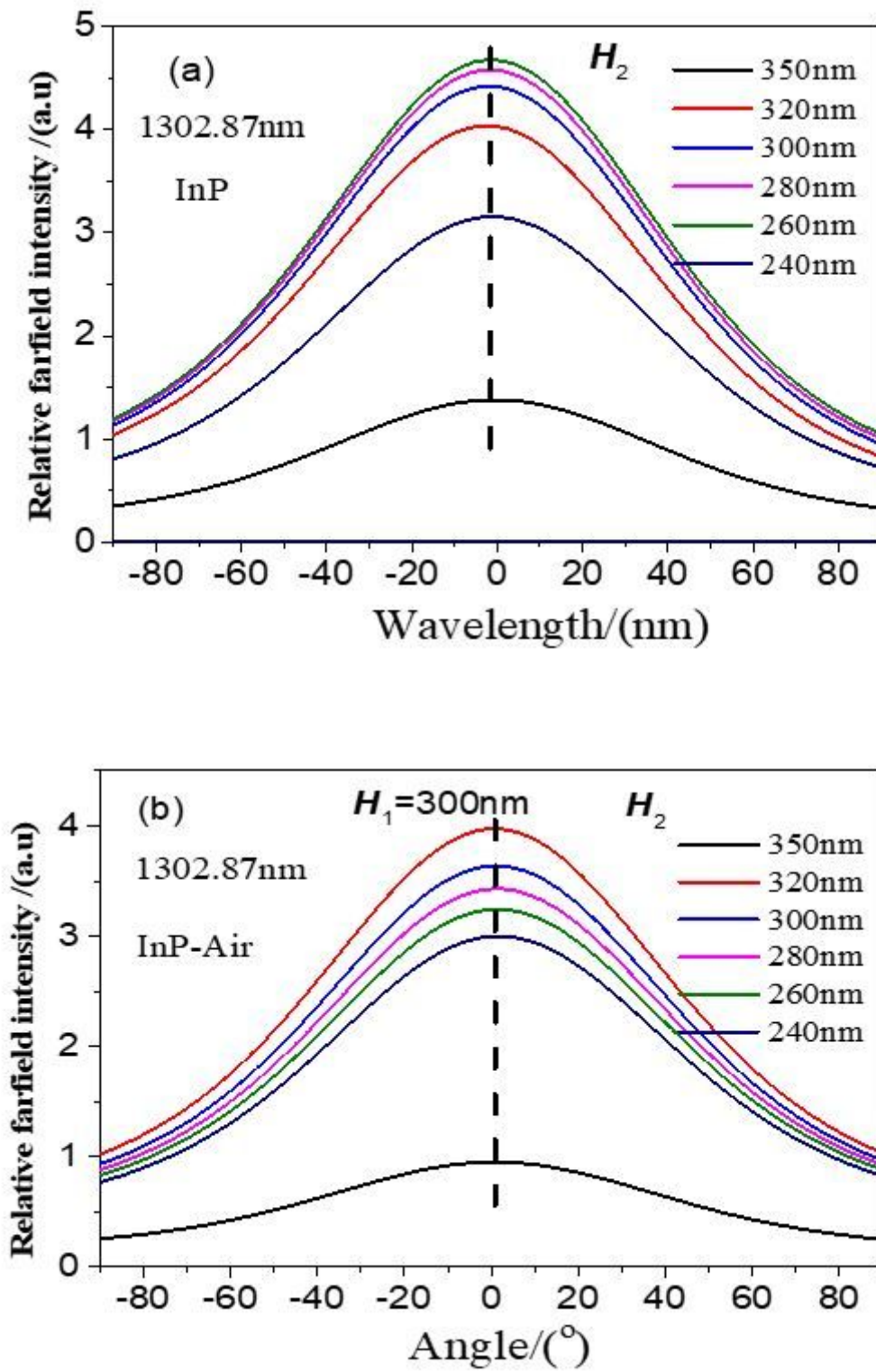Farfield with vavious angle from -90° to 90° and changeable height H2 from 240 nm to 350 nm before (a) and after (b) the addition of air cavity under 1302.87 nm monitoring.